Quaternary Science Reviews 259 (2021) 106888

Contents lists available at ScienceDirect

Quaternary Science Reviews

journal homepage: www.elsevier.com/locate/quascirev

High-frequency shifts in the Indian summer monsoon following termination of the YD event

Anil K. Gupta [a, 1, *], Raj K. Singh [b, 1], Som Dutt [c], Hai Cheng [d, e], Steven C. Clemens [f], Gayatri Kathayat [d]

[a] Department of Geology and Geophysics, Indian Institute of Technology Kharagpur, 721 302, India
[b] School of Earth, Ocean and Climate Sciences, Indian Institute of Technology Bhubaneswar, Odisha, 752050, India
[c] Wadia Institute of Himalayan Geology, 33 General Mahadeo Singh Road, Dehradun, 248 001, India
[d] Institute of Global Environmental Change, Xi'an Jiaotong University, Xi'an, 710049, China
[e] Department of Earth Sciences, University of Minnesota, Minneapolis, MN, 55455, USA
[f] Department of Earth, Environmental and Planetary Sciences, Brown University, Providence, RI, USA

A R T I C L E I N F O

Article history:
Received 10 May 2020
Received in revised form
2 March 2021
Accepted 3 March 2021
Available online 31 March 2021

Handling Editor: Mira Matthews

Keywords:
Indian summer monsoon
Younger Dryas
Bølling-Ållerød period
Abrupt wet and dry intervals
Umsynrang cave
Meghalaya

A B S T R A C T

High-resolution multi-proxy records are pivotal to analyze Indian monsoon variability and its linkages with socio-economic growth in South Asia. To constrain short-term shifts in the Indian monsoon, we analyzed a speleothem sample from Meghalaya, northeastern India encompassing ~15.4 to 10.1 kilo year before the Present (kyr BP). Our new speleothem data from Meghalaya suggests wet conditions in northeastern India during ~15.4 to 12.9 kyr BP and ~11.3 to 10.1 kyr BP, punctuated by a dry phase during ~12.9 to 11.3 kyr BP including the Younger Dryas (YD) cold interval. We suggest a southward shift of the Intertropical Convergence Zone (ITCZ) in addition to weak Atlantic Meridional Overturning Circulation and land-sea heat contrast during the YD event leading to a weak Indian summer monsoon. The Northern Hemisphere atmospheric heating shift the ITCZ northward, but our data shows high-frequency shifts in the ISM during ~11.3 to 10.1 kyr BP following termination of the YD cold event. This interval also shows a higher growth rate of the studied speleothem sample.

1. Introduction

The Younger Dryas (YD) was an abrupt climatic cold event that impacted the regional and global climates including the Indian monsoon system during ~12.9 to 11.6 kyr BP (before 1950 CE, hereafter; Dansgaard et al., 1989; Mayewski et al., 1993). The weakening of the Atlantic Meridional Overturning Circulation (AMOC) due to the sudden enhanced influx of freshwater into the North Atlantic has been suggested as a driver for the YD cold event (Partin et al., 2015; Schlolaut et al., 2017). In the Arctic, the YD terminated abruptly as marked by a sudden shift in the oxygen isotope ratios towards heavier values and reduction in dust concentration (Dansgaard et al., 1989). Both the Indian summer monsoon (ISM) and East Asian summer monsoon (EASM) show a pronounced weakening during YD (Wang et al., 2001; Yuan et al., 2004; Dutt et al., 2015; Cheng et al., 2020).

The ISM is dynamically linked to the latitudinal migration of the Inter-Tropical Convergence Zone (ITCZ) and high latitude climate events as possible drivers (Schulz et al., 1998; Gupta et al., 2003; Fleitmann et al., 2003; Yancheva et al., 2007). Numerous model and observational studies indicate weak ISM and EASM, and strong westerlies during the YD (Wang et al., 2001; Dutt et al., 2015; Lechleitner et al., 2017). Gupta et al. (2003) found teleconnections between millennial-scale cold events in the North Atlantic, better known as Bond events (Bond et al., 2001) and weakening of the ISM during the Holocene. The sun-climate link has been suggested playing a vital role in driving interannual to decadal-scale variability in the Earth's climate including the North Atlantic climate and the ISM (Neff et al., 2001; Shindell et al., 2001; Gupta et al., 2005, 2013). Late Pleistocene speleothem records from the Hulu and Dongge caves of China and Mawmluh cave of India indicate

* Corresponding author.
E-mail address: anilg@gg.iitkgp.ac.in (A.K. Gupta).
URL: https://doi.org/10.17632/9nsfnjnynb.1
[1] Formerly at Wadia Institute of Himalayan Geology, Dehradun.

https://doi.org/10.1016/j.quascirev.2021.106888
0277-3791/

centennial to millennial-scale changes in the EASM and ISM strength, respectively during the late Quaternary (Wang et al., 2001; Yuan et al., 2004; Dutt et al., 2015). Centennial-scale variability in ISM wind strength during the Ållerød interstadial was linked to intense solar irradiance (Gupta et al., 2013).

The ISM significantly impacts the socio-economic and cultural advancement in the Indian subcontinent. Extreme changes in the ISM thus impact human societies with economic and ecological implications owing to severe floods and droughts (Dutt et al., 2018, 2019, 2021; Gupta et al., 2019). It is therefore pertinent to understand the response of the ISM to abrupt climatic changes during cold and warm intervals in the late Quaternary. Speleothem based high resolution annual to interannual records of ISM precipitation is sparse, especially during the YD interval. Most of the high-resolution speleothem records from India are either younger (Berkelhammer et al., 2012) or older (Sinha et al., 2005) than the YD with an exception of a study by Dutt et al. (2015) and a discontinuous record by Lechleitner et al. (2017) from the Mawmluh cave Meghalaya. Speleothems from Meghalaya, northeastern Indian Himalaya hold promise to assess sub-decadal to centennial-scale Indian monsoon variability (Breitenbach et al., 2010; Berkelhammer et al., 2012; Dutt et al., 2015; Myers et al., 2015; Lechleitner et al., 2017; Huguet et al., 2018; Gupta et al., 2019) as the state receives ~75% of its annual rainfall during June, July, August and September (JJAS) also known as the summer monsoon season (Murata et al., 2007; Breitenbach et al., 2010). Annual rainfall amount in northeastern India does not show any significant negative or positive correlation with other regions of the Indian subcontinent (Parthasarathy et al., 1993). However long term variability of the ISM in northeastern India is quite similar to other regions of the Indian subcontinent as evidenced in proxy records showing early Holocene ISM strengthening, 4.2 ka weakening and so on (Berkelhammer et al., 2012; Dutt et al., 2015; Kathayat et al., 2018 and references therein). Stable isotopes of meteoric precipitation in the region and in turn the cave drip water is also biased towards the ISM as this season delivers most of the precipitation. A significant negative shift in $\delta^{18}O$ values of meteoric precipitation, river water and cave drip water is observed with the onset of ISM season and a positive shift is evident from November onwards following the summer monsoon season (Breitenbach et al., 2010, 2015; Lechleitner et al., 2017).

We have produced a high-resolution record of ISM variability using stable oxygen isotope ratio from a speleothem sample UMS-1 of Umsynrang cave, Meghalaya to understand sub-decadal to centennial-scale ISM variability during ~15.4 to 10.1 kyr BP encompassing the YD cold event (Fig. 1). Further, we have correlated YD and early Holocene data with high resolution published speleothem records from the Mawmluh cave, Meghalaya situated near Umsynrang cave (Fig. 1; Berkelhammer et al., 2012), Hulu and Dongge Cave records of EASM variability (Fig. 1; termed as Chinese cave; Cheng et al., 2009, 2016), Palawan cave, western Philippines reflecting western Pacific variability (Fig. 1; 10.2°N and 118.9°E; Partin et al., 2015; not during early Holocene), Liang Luar cave, Indonesia reflecting Australian-Indonesian monsoon rainfall (Fig. 1; 8° 32′N, 120° 26′E; Griffiths et al., 2009), and Sofular cave, Turkey (Fig. 1; 41°25′N, 31°56′E; Fleitmann et al., 2009) reflecting mid-latitude Northern Hemisphere (NH) precipitation. Further to investigate the role of sea surface temperature (SST) during the YD and early Holocene, we have correlated our data with reconstructed SST of Malabar Coast, eastern Arabian Sea (Fig. 1; SK237-GC04; 10° 58.65′N, 74° 59.96′E; Saraswat et al., 2013), western Bay of Bengal (Fig. 1; MD 161/17; 16° 03.63′N, 82° 01.29′E; Panmei et al., 2017) and western equatorial Pacific (Fig. 1; MD98-2188; 14° 82′N, 123° 49′E Dang et al., 2012, data modified at NOAA site on 06-05-2020).

2. Material and methods

A 319 mm long inactive stalagmite sample (UMS-1) was collected from the Umsynrang cave (25°13′N, 92°21′E; 825 m asl), ~25 Km SE of Jowai Meghalaya, northeastern India from a narrow chamber around ~300 m inside the cave entrance (Fig. 2). Umsynrang cave is a 5.6 Km long network of caves in a scarcely populated area (Kharpan Daly, 2006; Breitenbach, 2009) rich in active and inactive stalagmites found at different levels (Fig. 2). The limestone host rock of the middle Eocene Jaintia Group is overlain by ~40 m sandstone intercalated by a 50 cm thick coal seam. The vegetation over the cave consists of both grassland and tropical evergreen forests (Breitenbach, 2009). The chamber has almost a hundred percent relative humidity and a stable temperature of around 20.6 ± 0.6 °C (Breitenbach, 2009). The sample was split into two halves, polished and subsampled for analysis.

A total of nine ^{230}Th dates were obtained using Thermo Finnigan ‘Neptune’ multi-collector inductively coupled plasma mass spectrometry at the Department of Earth Sciences, University of Minnesota, USA following the procedure described by Cheng et al. (2013; Table 1). The age model has been established using the StalAge package (Scholz and Hoffmann, 2011) in R-software (Fig. 3; R Core Team, 2017). The $\delta^{18}O$ measurements were carried out for

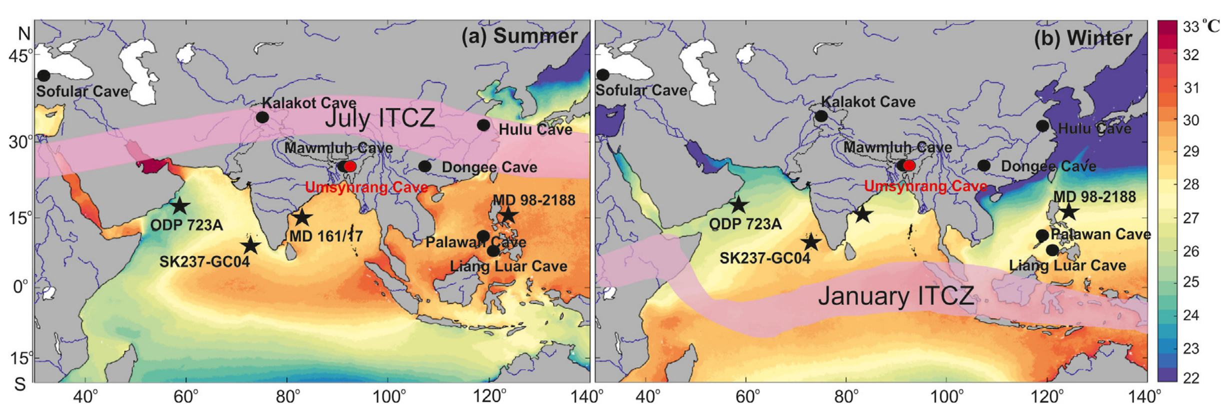

Fig. 1. Location of Umsynrang cave, Meghalaya (Red dots) along with the locations of Mawmluh cave Meghalaya, India, Hulu and Dongge caves of China, Palawan cave, western Philippines, Liangluar cave, Indonesia, and Sofular cave, Turkey (Black dots). The position of ODP Hole 723A (Gupta et al., 2013), Core sites SK 237-GC-04 (Saraswat et al., 2013), MD 164/17 (Panmei et al., 2017) and MD 98-2188 (Dang et al., 2012) are marked by black stars, (a) Mean Summer Sea Surface Temperature (b) Mean Winter Sea Surface Temperature (2002–2018; Source: NASA, MODIS). The colour bar on the right side represents the temperature scale in °C. The light pink colour shaded portion is the position of the Intertropical Convergence Zone (ITCZ). (For interpretation of the references to colour in this figure legend, the reader is referred to the Web version of this article.)

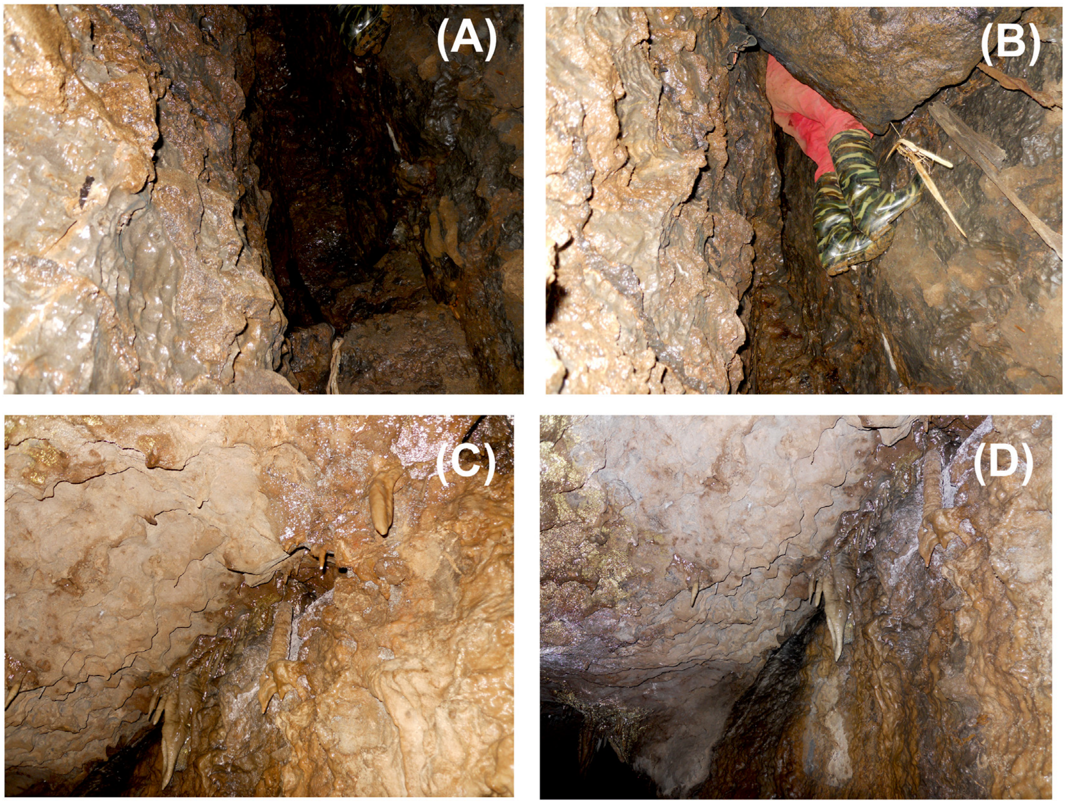

Fig. 2. (A) & (B) - Narrow vertical entrance of the Umsynrang cave, Meghalaya, India. (C) & (D) - Chamber inside the Umsynrang cave, from where UMS-1 samples were collected.

Table 1
^{230}Th dating results of stalagmite UMS-1 from the Umsynrang cave, Meghalaya India. The ages are reported with 2σ uncertainty.

Sample Number	Depth (mm)	^{238}U (ppb)	^{232}Th (ppt)	^{230}Th/^{232}Th (atomic x10^{-6})	δ^{234}U (measured)	^{230}Th/^{238}U (activity)	^{230}Th Age (yr) (uncorrected)	^{230}Th Age (yr) (corrected)	δ^{234}U$_{Initial}$ (corrected)	^{230}Th Age (yr BP) (corrected)
UMS-1-8	6 ± 1	1535 ± 3	613 ± 13	3604.4 ± 77.1	−18.2 ± 1.9	0.0873 ± 0.0003	10155 ± 43	**10143 ± 44**	−19 ± 2	**10081 ± 44**
UMS-1-1	19 ± 1	1257 ± 3	2166 ± 43	859 ± 18	−28.1 ± 1.6	0.0877 ± 0.0005	10312 ± 69	**10261 ± 78**	−29.2 ± 2	**10198 ± 78**
UMS-1-2	50 ± 1	1402 ± 2	1815 ± 37	1119 ± 24	−25.9 ± 1.6	0.0879 ± 0.0004	10312 ± 58	**10273 ± 64**	−27 ± 2	**10210 ± 64**
UMS-1-3	78 ± 1	1245 ± 2	1748 ± 36	1057 ± 22	−17.9 ± 1.7	0.0901 ± 0.0005	10492 ± 64	**10451 ± 71**	−18 ± 2	**10388 ± 71**
UMS-1-4	151 ± 1	1191 ± 2	1199 ± 25	1489 ± 32	−45.9 ± 1.5	0.0910 ± 0.0005	10939 ± 65	**10908 ± 68**	−47 ± 2	**10845 ± 68**
UMS-1-5	207 ± 1	1334 ± 3	3842 ± 78	533 ± 11	−43.4 ± 1.7	0.0932 ± 0.0005	11183 ± 64	**11095 ± 89**	−45 ± 2	**11032 ± 89**
UMS-1-6	263 ± 1	9066 ± 19	1619 ± 34	9778 ± 206	−39.6 ± 1.5	0.1059 ± 0.0003	12747 ± 43	**12747 ± 44**	−41 ± 2	**12685 ± 44**
UMS-1-7	289 ± 1	1551.4 ± 7.3	1117 ± 23	2620 ± 56	−37.3 ± 3.4	0.1144 ± 0.0007	13806 ± 109	**13784 ± 110**	−39 ± 4	**13722 ± 110**
UMS-1-9	310 ± 1	6235 ± 36.3	5993 ± 125	2212 ± 48	−25.5 ± 2.9	0.1289 ± 0.0011	15487 ± 146	**15458 ± 148**	−27 ± 3	**15396 ± 148**

318 subsamples, which were sampled at every 1 mm interval, and analyzed at Brown University, USA using MAT 252 equipped with Kiel carbonate III system. Out of these 318 samples, 264 samples are from 12.6 to 10.1 kyr representing YD and early Holocene intervals with an age resolution of ~9.5 yr per sample, which increases to ~46 yr in the samples in the interval older than the YD. The in-house standards of Carrara marble (n = 58) and Blue Yale marble (n = 31) were analyzed repeatedly during the analysis showing a precision (1s) of 0.05 and 0.06‰, respectively. The results are reported against the VPDB standard in standard delta (δ) notation (Fig. 4i, ii).

The speleothem δ^{18}O data of Umsynrang cave (this study), Mawmluh cave, Chinese cave record (Dongge and Hulu cave), Liang Luar cave, and Sofular cave have continuous record between 12.4 and 10.1 kyr BP with an age resolution of less than 9 yr except for Chinese cave where it is 11.8 yr per sample (Fig. 5). The Palawan cave has a continuous record up to 10.8 kyr BP with an age resolution of less than 9 yr and hence not considered for analysis during the early Holocene. The reconstructed SST record of the eastern Arabian Sea (EAS), western Bay of Bengal (BoB) and western Pacific (WP) have a resolution of ~60–70 yr (Fig. 6). Hence to assess the statistical similarity in these cave records and their relationship with the SST of EAS, BoB and WP during the YD and early Holocene, a separate Pearson Correlation and Principal Component Analysis (PCA) were performed for the period between 12.4 and 11.3 kyr BP (Fig. 7) and between 11.3 and 10.1 kyr BP except for Palawan cave (Fig. 8). These data were linearly interpolated for 10 years interval using Analyseries software (Paillard et al., 1996) prior to Pearson Correlation and Principal Component Analysis (PCA) using FactoMineR package in R-software (Das et al., 2021; Dutt et al., 2021; Kassambara, 2017; Lê et al., 2008; R Core Team, 2017, Tables 1s, 2s, 3s, 4s). PCA biplot variables (Caves δ^{18}O and SST) is further grouped using K-mean clustering algorithm using the same package (Figs. 7 and 8; Das et al., 2021; Dutt et al., 2021; Kassambara, 2017). The individual Cos2 and Contribution of dimension 1 (Dim 1 or PC1) and dimension 2 (Dim 2 or PC2) were plotted against time-series to

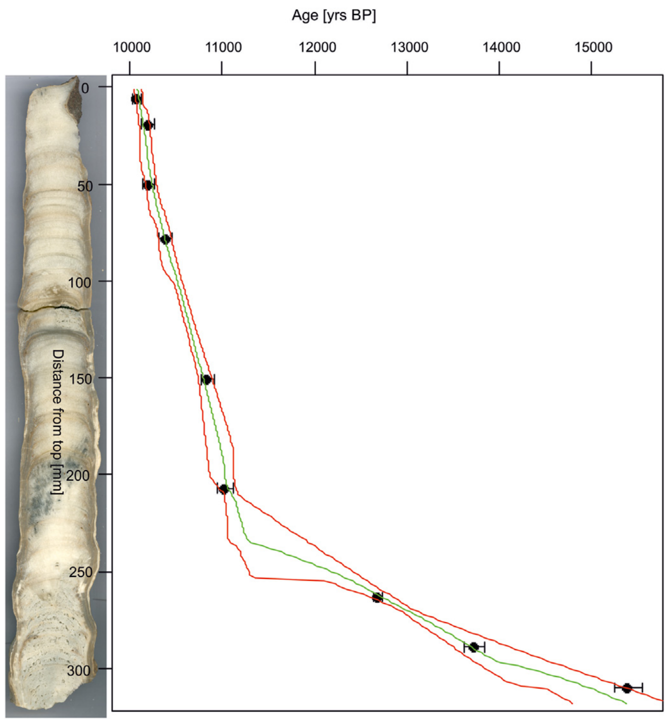

Fig. 3. Age-Depth relation of Stalagmite UMS-1 from the Umsynrang cave, north-eastern India. Half cut section of UMS-1 stalagmite.

assess their variability with time (Figs. 9 and 10). The Cos2 is the quality representation of an individual on the factor map and calculated as the squared coordinates. The high Cos2 indicates a good representation of individual on the Principal Component and the value of Cos2 is between 0 and 1. The individual contribution to the Principal Component (in percentage), which sum to 100 is also plotted against time series (Lé et al., 2008; Kassambara, 2017).

3. Results and interpretation of proxy data

The U–Th measurements of nine subsamples of stalagmite UMS-1 indicate an age uncertainty of less than 90 yr (2σ), except for the bottom two ages (Table 1). The age-depth model suggests continuous growth of UMS-1 between ~15.4 and 10.1 kyr BP (Fig. 3). The collected stalagmite formation ceased at 10.1 kyr BP and did not preserve the younger record. There is no hiatus visible in the deposition of the stalagmite sample, and high variations occurred in the growth rate because of significant shifts in the regional climate (Fig. 3).

The $\delta^{18}O$ of sample UMS-1 varies from −6.56 to −4.94‰ between ~15.4 and 10.1 kyr BP (Fig. 4ii). This variability is almost similar to an earlier record from the Mawmluh cave by Berkelhammer et al. (2012), Dutt et al. (2015), Lechleitner et al. (2017) and Huguet et al. (2018) during the same interval (Fig. 4iii). The drip water isotope behaviour depends on the thickness of the overburden and vegetation above the cave (Lechleitner et al., 2017). The individual cave temperature and CO_2 also affect the drip water $\delta^{18}O$ value, which is reflected in the stalagmite record (Breitenbach et al., 2015). The $\delta^{18}O$ values in different chambers of Umsynrang cave are between −6.8 and −5.2‰, while $\delta^{18}O$ value in different chambers of Mawmluh cave is between −5.5 and −7.7‰, (Breitenbach et al., 2015; Tiwari et al., 2015). The Mawkhyrdop river water before entering the Mawmluh cave has a $\delta^{18}O$ value of −6.4‰ (Tiwari et al., 2015). After long term (2007–2013) seasonal observation of Mawmluh cave, Breitenbach et al. (2015) concluded that drip water $\delta^{18}O$ is closely related to monsoon rainfall, but vary at a seasonal scale. Hence $\delta^{18}O$ of individual speleothem has different values within the range, but have an almost similar trend. Further, the Mawmluh cave is situated around 400 m above the level of the Umsynrang cave and imparts more negative isotope ratios to the meteoric precipitation at Mawmluh cave and in turn the drip water and speleothems in the cave.

The $\delta^{18}O$ in speleothems, deposited in isotopic equilibrium, reflects the isotopic signature of regional precipitation, which in itself is influenced by changes in moisture source, distance travelled by moisture, amount of precipitation and freshwater plume in the Bay of Bengal (Breitenbach et al., 2010, 2015; Gupta et al., 2019). All these processes relate lighter oxygen isotope ratios with higher rainfall (Breitenbach et al., 2015; Dutt et al., 2015, 2021; Kathayat et al., 2018; Lechleitner et al., 2017). We interpret changes in the speleothem $\delta^{18}O$ value as variations in the isotopic composition of source waters and processes occurring along transport pathways, all of which, in turn, reflect changes in the ISM strength. Different phases are observed in the $\delta^{18}O$ time series of UMS-1, (i) the $\delta^{18}O$ value are generally depleted between 15.4 and 12.9 kyr BP varying from −6.56 to −5.69‰, the least value centred at ~14.8 kyr BP, (ii) at ~12.9 kyr BP there is a sudden enrichment in the oxygen isotope ratio which ended at ~11.3 kyr BP, and (iii) following ~11.3 kyr BP the $\delta^{18}O$ values show depletion until 10.1 kyr BP with high-frequency shifts (Fig. 4ii and 5i). The $\delta^{13}C$ value of the Meghalaya cave is generally similar to $\delta^{18}O$ reflecting local hydroclimatic condition and suggesting a weak/strong ISM in the Meghalaya cave (Lechleitner et al., 2017). However, the $\delta^{13}C$ in Umsynrang cave shows heavier values during and prior to YD event. During the early Holocene conditions reversed with lighter $\delta^{13}C$ values corresponding with strong ISM and heavier $\delta^{13}C$ values corresponding with the period of weak ISM (Fig. 4i).

Hendy test suggests a non-significant relationship between speleothem $\delta^{13}C$ and $\delta^{18}O$ values indicating that the isotopic signature of speleothem has not been affected by the kinetic fractionation due to changes in cave temperature, ventilation or carbonate precipitation in soil horizon before the speleothem deposition, etc. (Hendy, 1971; Dreybrodt, 2008). The correlation between $\delta^{13}C$ and $\delta^{18}O$ of sample UMS-1 shows no significant correlation ($r = 0.16$), suggesting that isotopic signatures of this sample primarily reflect isotopic equilibrium with the meteoric precipitation and hence regional climatic signal (Fig. 11; Hendy, 1971; Dreybrodt, 2008; Wiedner et al., 2008).

Pearson Correlation Coefficient analysis of speleothem $\delta^{18}O$ value of UMS-1 shows a positive correlation with the Mawmluh and Chinese caves, and a negative correlation with the Palawan and Liang Luar caves, WP and EAS SST during 12.4 to 11.3 kyr BP. No significant correlation between UMS-1 and BoB SST has been observed (Table 1s). The correlation is similar during 11.3–10.1 kyr BP, except that Liang Luar cave has a positive correlation during this interval and no significant correlation with any SST record (Table 2s). The PCA analysis for the period between 12.4 and 11.3 kyr BP extracted two factors that explain 73% of data variance (Table 3s). The PCA biplot variables grouped using K-mode clustering are suggesting three groups. Umsynrang, Mawmluh and Chinese caves having a positive score on PC-1 form the 1st group, Sofular cave and BoB SST having a negative score on PC-2 form the 2nd group and the Palawan and Liang Luar caves along with EAS and WP SST form the 3rd group having negative scores on PC-1 (Fig. 7; Table 3s). The PCA analysis for the period between 11.3 and 10.1 kyr BP also extracted two factors that explain just 58% of the data variance (Table 4s). Umsynrang, Mawmluh, Chinese and Liang Luar caves having a positive score on PC-1 form the 1st group, BoB and EAS SST having a negative score on PC-2 form the 2nd group and the Sofular cave along with WP SST form the 3rd group

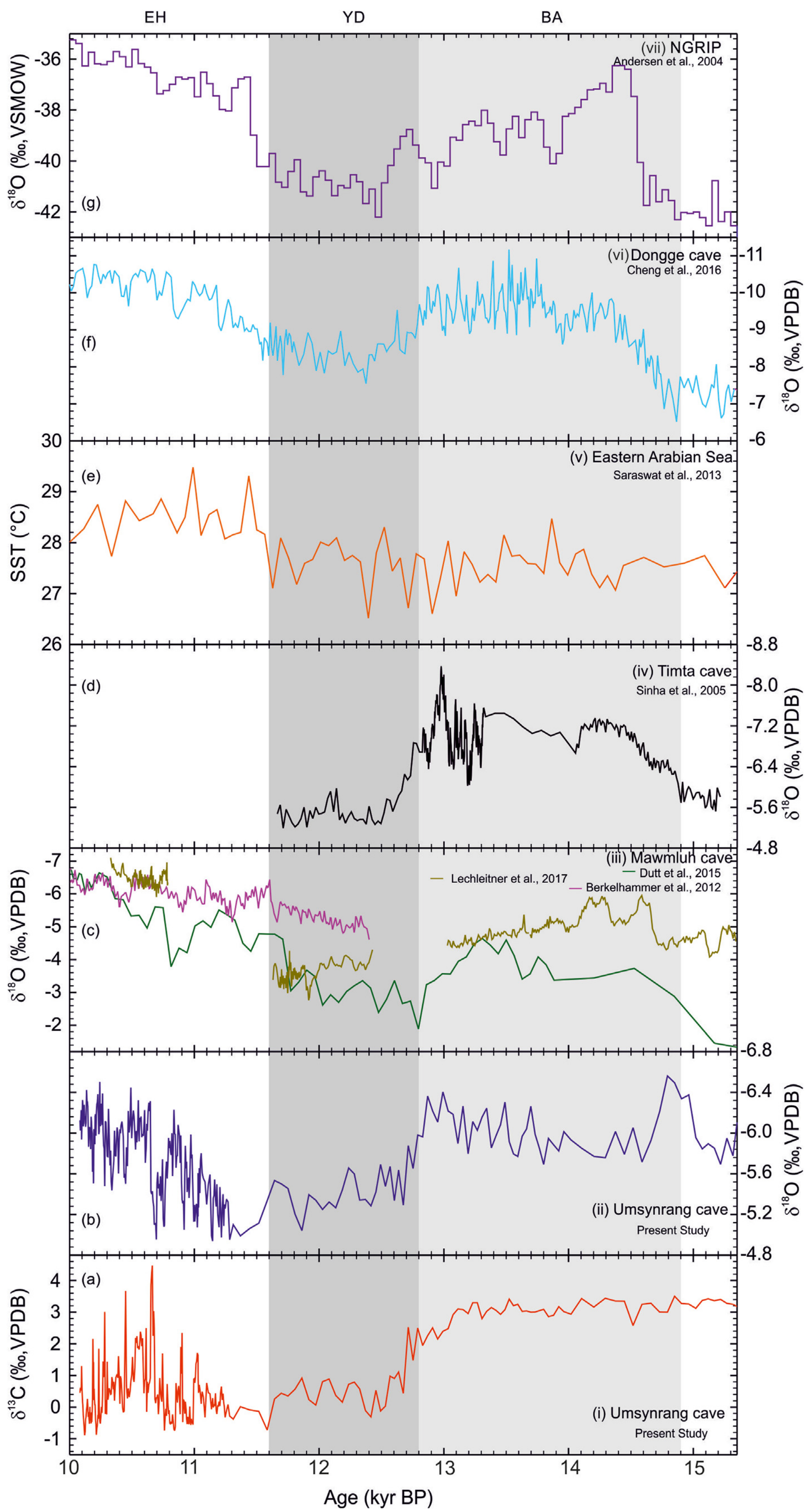

Fig. 4. Comparison of Umsynrang cave $\delta^{18}O$ records for the period 15.5 to 10 kyr BP with other proxy records. (i) $\delta^{13}C$ time series from the Umsynrang cave (present study), (ii) $\delta^{18}O$ time series from the Umsynrang cave (present study), (iii) $\delta^{18}O$ time series of ISM variability from the Mawmluh cave (Berkelhammer et al., 2012; Dutt et al., 2015; Lechleitner et al., 2017), (iv) $\delta^{18}O$ time series for ISM variability from the Timta cave (Sinha et al., 2005), (v) Paleo sea surface temperature in the eastern Arabian Sea (Saraswat et al., 2013), (vi) $\delta^{18}O$ time series from the Dongge cave (Cheng et al., 2016), and (vii) $\delta^{18}O$ record from North Greenland Ice Core Project (NGRIP, 2004). The shaded bar indicates Bølling-Ållerød (BA) and Younger Dryas (YD) intervals.

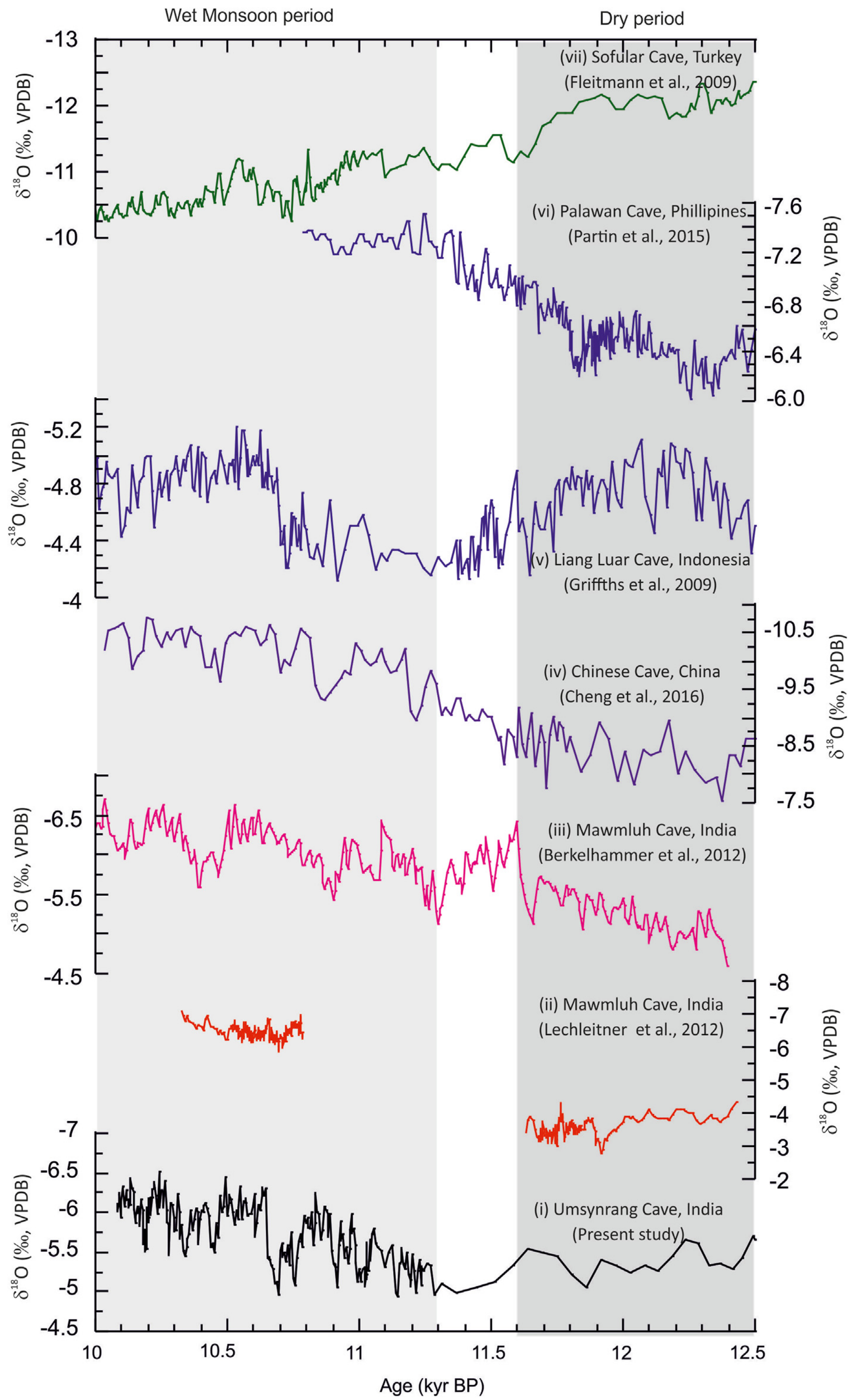

Fig. 5. Comparison of Umsynrang cave $\delta^{18}O$ records for the period 12.5 to 10 kyr BP with other proxy records. (i) Umsynrang cave $\delta^{18}O$, (ii, iii) Mawmluh cave, India $\delta^{18}O$, (iv) Chinese cave $\delta^{18}O$ (combined Hulu and Donge cave), (v) Liang Luar cave Indonesia, $\delta^{18}O$ (vi) Palawan cave, Philippines $\delta^{18}O$ and (vii) Sofular cave, Turkey $\delta^{18}O$. The light shaded bar indicates wet and dark shaded bar indicates the dry periods and the unshaded portion indicates a continuation of the dry period following the termination of the YD.

having negative scores on PC-1 (Fig. 8; Table 4s). The time series plot of Dim 1 Cos2 is exhibiting a low amplitude periodic shift with a declining trend between 12.4 and 11.6 kyr BP, which sharply increases and has a very high value between 11.6 and 11.3 kyr BP (Fig. 9). The Dim 2 Cos2 is exhibiting high amplitude variability between 12.4 and 11.6 kyr BP and has a low value between 11.6 and 11.3 kyr BP (Fig. 9). The contribution of Dim 1 and Dim 2 is maximum between 11.6 and 11.3 kyr BP and between 12.4 and 12.2 kyr BP, respectively (Fig. 9). For the period between 11.3 and 10.1 kyr BP, both Dim 1 and Dim 2 Cos2 values are exhibiting very high

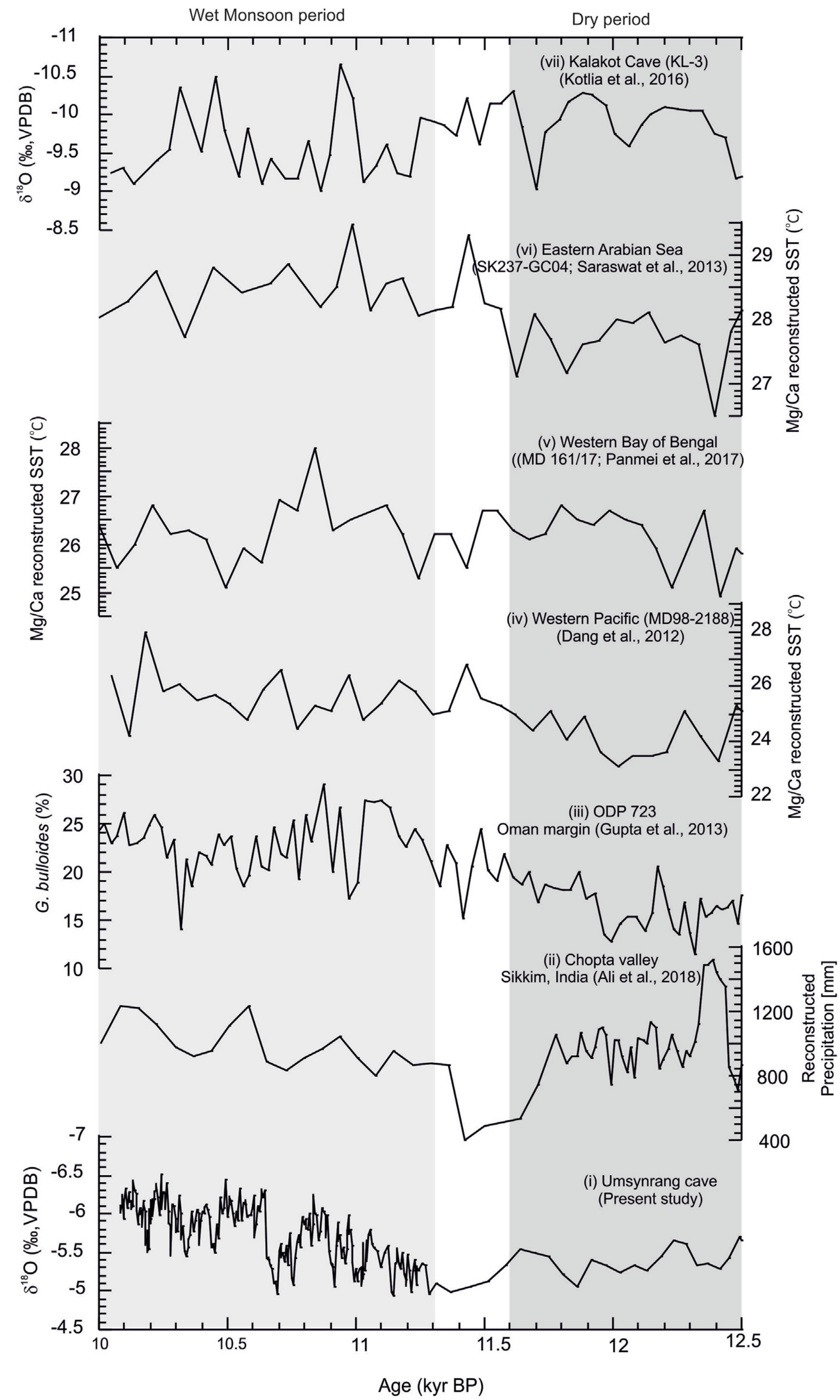

Fig. 6. Comparison of Umsynrang cave $\delta^{18}O$ records for the period 12.5 to 10 kyr BP with other proxy and paleo sea surface temperature (SST) records. (i) Umsynrang cave $\delta^{18}O$, (ii) Reconstructed paleo precipitation in the eastern Himalaya (Chopta valley; Ali et al., 2018), (iii) Upwelling indicator species *G. bulloides* abundance at ODP Hole 723A (Gupta et al., 2013), (iv) Western Pacific paleo SST (Dang et al., 2012, modified data at NOAA site on 16/05/2020), (v) Paleo SST at western Bay of Bengal (Panmei et al., 2017), (vi) Paleo SST in the eastern Arabian Sea (Saraswat et al., 2013) and (vii) Kalakot cave, India $\delta^{18}O$ (Kotlia et al., 2016) influenced by westerly winds. The light shaded bar indicates wet and dark shaded bar indicates dry periods whereas the unshaded portion indicates a continuation of the dry period following termination of the YD.

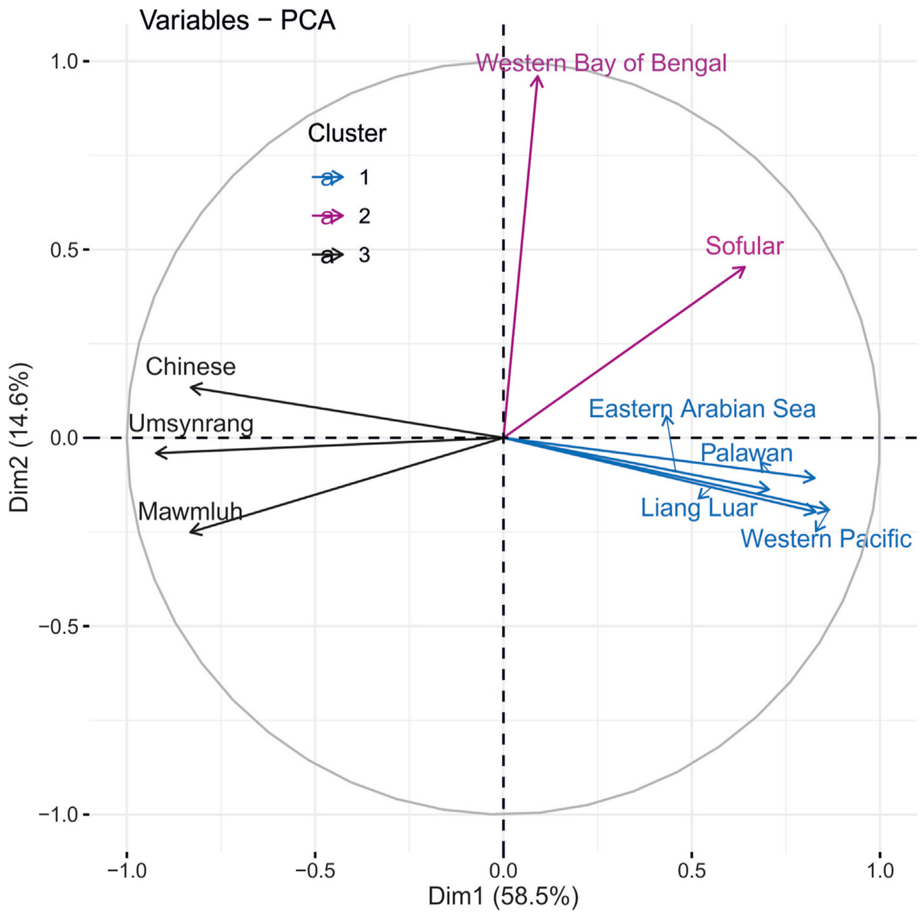

Fig. 7. Principal Component Analysis (PCA) biplot for YD (12.4–11.3 kyr BP) (i) Umsynrang cave $\delta^{18}O$, (ii) Mawmluh cave, India $\delta^{18}O$, (iii) Chinese cave $\delta^{18}O$ (combined Hulu and Donge cave), (iv) Liang luar cave Indonesia, $\delta^{18}O$ (v) Palawan cave, Philippines $\delta^{18}O$, (vi) Sofular cave, Turkey $\delta^{18}O$ (vii) Western Pacific SST, (viii) Western Bay of Bengal SST (ix) Eastern Arabian Sea SST were grouped using k-means cluster analysis.

amplitude periodic variability and contribution is low except for a few intervals (Fig. 10).

4. Discussion

4.1. Pre YD period (~15.4–12.9 kyr BP)

The varying but lighter $\delta^{18}O$ values (−6.56 to −5.69‰) between 15.4 and 12.9 kyr BP suggest strong and variable summer monsoon conditions in the study region. Our record could not constrain Bølling-Ållerød (B-A) interval distinctly due to low sample resolution owing to decreased carbonate deposition during 15.4 and 12.9 kyr BP (Fig. 4ii). However, numerous proxy records have earlier suggested extreme ISM conditions during warm and moist interstadial Bølling-Ållerød (B-A) interval following Henrich interstadial-1 driven by the rapid rise of CO_2 in the atmosphere and release of heat from the deep North Atlantic (Köhler et al., 2011; Gupta et al., 2013; Thiagarajan et al., 2014; Dutt et al., 2015). The convective activities enhanced during the B-Å interstadial in the tropics, resulting in a northward shift of the ITCZ that led to an increase in summer precipitation across the Indian subcontinent (Dykoski et al., 2005; Cheng et al., 2009; Gautam et al., 2019). The period between 14.6 and 12.9 kyr BP is marked by higher precipitation in Timta, Hulu and Dongge cave records as well as at Arabian Sea ODP Hole 723A (Fig. 4ii, 4iv; Yuan et al., 2004; Gupta et al., 2013; Sinha et al., 2005) except for few intervals of a cold period during the Ållerød period. Gupta et al. (2013) argued that the stronger westerly winds and southward shift of the ITCZ during the cold intervals due to increased latitudinal thermal gradient led to the weakening of the ISM. Several other paleoclimatic records from the Indian subcontinent and other nearby regions also suggest overall increased precipitation between 15 and 12.9 kyr BP and sudden weakening of the summer monsoon during the cold Ållerød period (Thompson et al., 2000; Gupta et al., 2013; Dutt et al., 2015; Rawat et al., 2015).

4.2. The YD period (~12.9–11.3 kyr BP)

An abrupt enrichment in the oxygen isotope ratio at ~12.9 kyr BP indicates a weakening of the ISM and decreased summer precipitation in northeastern India at the onset of the YD cold interval. Earlier studies from the Mawmluh cave (Figs. 4iii, 5ii, 5iii; Berkelhammer et al., 2012; Dutt et al., 2015; Lechleitner et al., 2017), Timta cave (Fig. 4iv; Sinha et al., 2005), Tso Kar and Tso Moriri lakes (Mishra et al., 2015; Wünnemann et al., 2010), and Chandra peat bog of northwestern Himalaya (Rawat et al., 2015) also suggest an abrupt decrease in precipitation around 12.9 kyr BP. The reconstructed precipitation for the eastern Himalaya also shows a weak ISM during the YD and weakest between ~11.7 and 11.4 kyr BP (~63% drop in rainfall) followed by an abrupt increase in ISM precipitation (Fig. 6ii; Ali et al., 2018). A similar decline in EASM precipitation has also been observed (Fig. 4vi, 5iv; Cheng et al., 2016). The decrease in ISM precipitation coincides with the weakening of the AMOC, which caused sea-ice expansion and a lowering

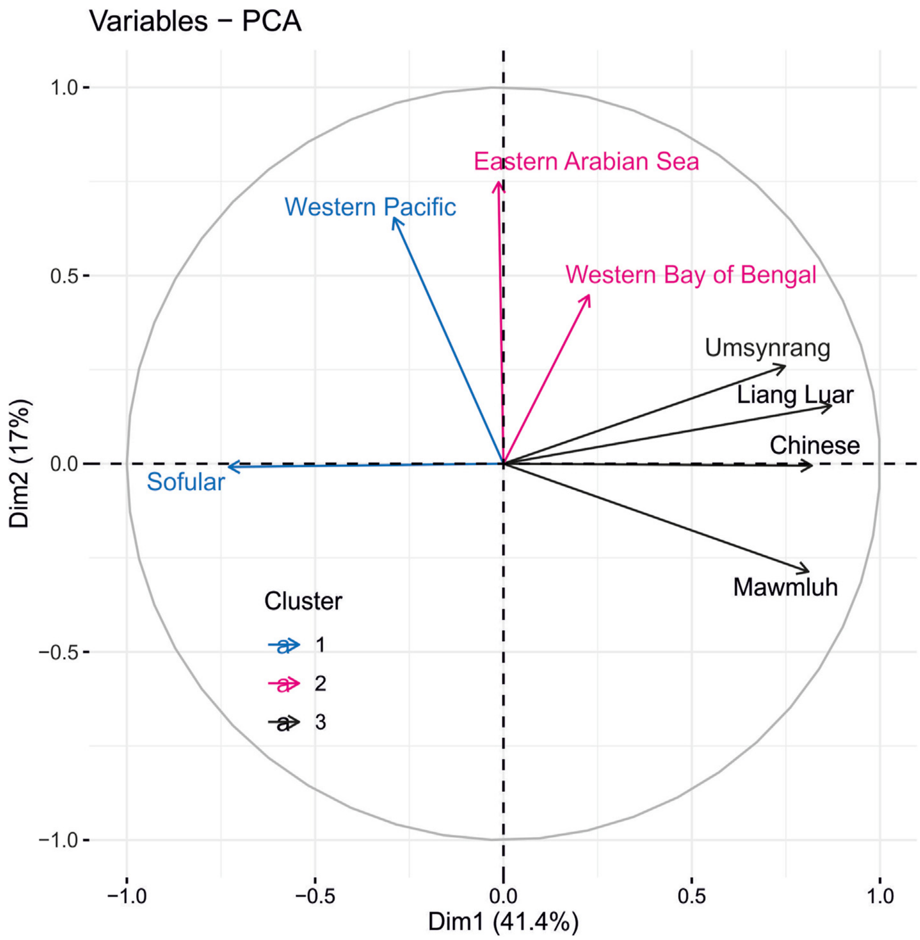

Fig. 8. Principal Component Analysis (PCA) biplot for the early Holocene (11.3–10.1 kyr BP) (i) Umsynrang cave $\delta^{18}O$, (ii) Mawmluh cave, India $\delta^{18}O$, (iii) Chinese cave $\delta^{18}O$ (combined Hulu and Donge cave), (iv) Liang Luar cave Indonesia, $\delta^{18}O$ (v) Sofular cave, Turkey $\delta^{18}O$ (vi) Western Pacific SST, (vii) Western Bay of Bengal SST (viii) Eastern Arabian Sea SST were grouped using k-means cluster analysis.

of temperature in the NH (Condron and Winsor, 2012). The glacier expansion in the NH weakens the ISM through increased strength of the mid-latitude westerlies and their downwind effect in South Asia (Fig. 6vii; Gupta et al., 2003, 2005; Dutt et al., 2015; Kotlia et al., 2016).

The YD is poorly understood due to the lack of high-resolution proxy records spanning YD or owing to poor chronology or hiatus (Lechleitner et al., 2017; Kotlia et al., 2016). Recently, Cheng et al. (2020) suggested fast propagation of North Atlantic change via meridional migration of ITCZ, Hadley circulation and the westerly jet stream. We have tried to assess the detailed mechanism of a weak monsoon during the YD by comparing UMS-1 records with other tropical and mid-latitude NH cave records (Fig. 5) and SST over WP, EAS and BoB (Fig. 6). The two tropical speleothem records from the Palawan (Partin et al., 2015) and Liang Luar caves (Griffths et al., 2009) have an inverse relationship with the Umsynrang cave record during the YD (Figs. 5 and 7; Table 1s). The Liang Luar cave record shows increased summer precipitation during the YD cold event, which was linked to the migration of the ITCZ to the equator (Griffiths et al., 2009). The Palawan cave record suggests relatively drier conditions during the YD as represented by a smaller increase in stalagmite $\delta^{18}O$ values (Partin et al., 2015). However, PCA analysis, K-means clustering of variables (caves) in PCA biplot (Fig. 7) and Pearson Correlation (Table 1s) suggest similarities between the Palawan and Liang Luar cave records. The Umsynrang, Mawmluh and Chinese cave records suggest a weak ISM during the YD cold event. The PCA analysis, K-means clustering of variable of PCA biplot (Fig. 7) and Pearson Correlation of stalagmite $\delta^{18}O$ also suggest similar monsoon behaviour in these cave records (Table 1s).

Palawan and Liang Luar cave $\delta^{18}O$ has a negative correlation with Umsynrang, Mawmluh and Chinese cave $\delta^{18}O$ and has an opposite PCA loading in PC 1 (Fig. 7, Table 1s) suggest a periodic shift in the ITCZ between 12.4 and 11.6 kyr BP towards the equator or SH (Fig. 9). The periodic shift in the ITCZ towards the equator caused higher rainfall at Liang Luar during the YD interval. Sofular cave $\delta^{18}O$ also shows a negative correlation with Umsynrang, Mawmluh and Chinese cave $\delta^{18}O$ values as the Sofular cave may receive higher precipitation due to strengthened westerlies or moisture source may be from the Black Sea (Fleitmann et al., 2009). During the late Pleistocene dominant source of moisture to Sofular cave was the Black Sea (Fleitmann et al., 2009). The EAS and WP SST records are closely associated with Palawan and Liang Luar cave $\delta^{18}O$ record and negatively correlated with the Umsynrang, Mawmluh and Chinese cave $\delta^{18}O$ values (Fig. 7). The western BoB exhibits overall warming during the YD (~1.8 °C; Fig. 6; Panmei et al., 2017) and not significantly correlated either with Umsynrang and Chinese cave $\delta^{18}O$ values or Palawan and Liang Luar cave $\delta^{18}O$ values, but has a poor negative correlation with Mawmluh cave $\delta^{18}O$ values and has a weak positive correlation with the Sofular cave $\delta^{18}O$ values (Fig. 7, Table 1s). Panmei et al. (2017) proposed that the Northern Indian Ocean did not cool significantly during the YD due to the weakening of the AMOC. The YD duration observed in

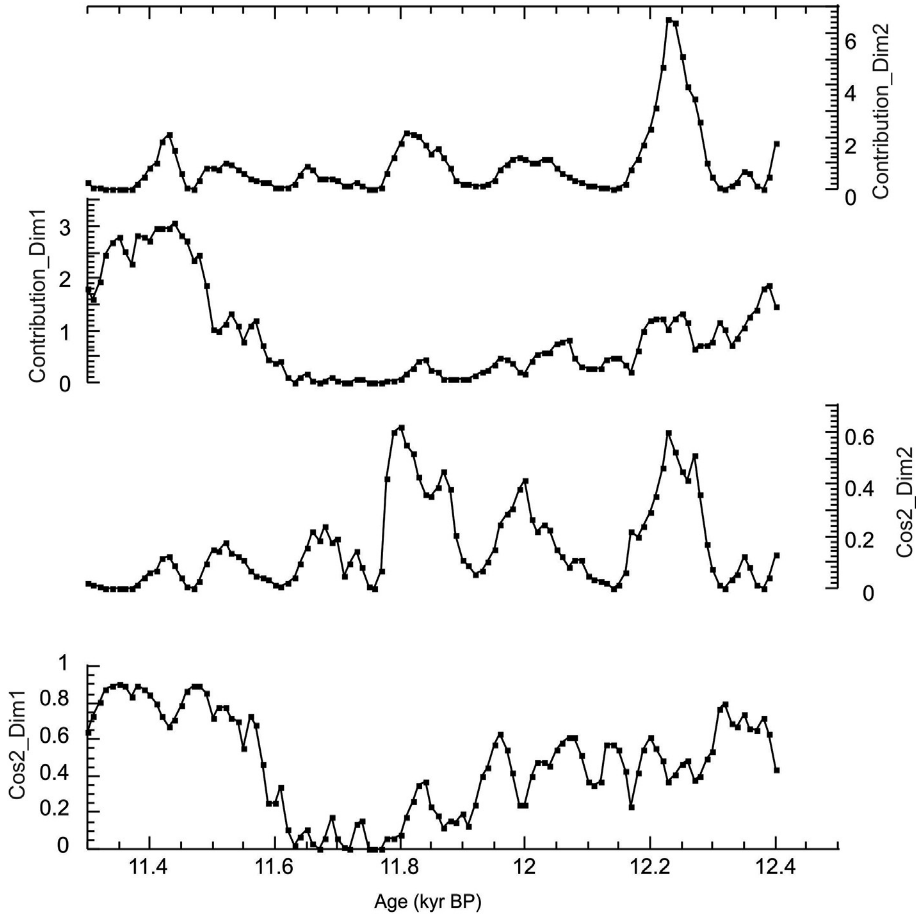

Fig. 9. The time series plot of Cos2 and Contribution value of dimension 1 (Dim1 or PC1) and dimension 2 (Dim2 or PC2) for the period between 12.4 and 11.3 kyr BP.

the Kalakot cave is between 12.7 and 12.2 kyr BP as the cave location is influenced by the westerlies (Fig. 6vii; Kotlia et al., 2016). The stronger westerlies did not allow heating of the northern Indian subcontinent landmass, and as a result, it has not created enough pressure difference for continent ward flowing ISM wind. The weakening of the AMOC decreased upwelling in the western Arabian Sea marked by the low abundance of upwelling indicator species *G. bulloides* (Fig 6iii; Gill et al., 2017; Gupta et al., 2013), which in turn further supports weak monsoonal wind during the YD. However, all these changes have a periodic variation and declining effect between 12.4 and 11.6 kyr BP (Fig. 9). The combined effect of AMOC weakening and westerlies jet stream have periodically moved the ITCZ southward, added with reduced land-sea heat contrast cause lower monsoonal precipitation during the YD.

The termination of the YD cold interval at ~11.3 kyr BP at Umsynrang cave roughly coincides with the standard termination age of the YD event at 11.6 kyr BP. This was followed by a sudden strengthening of the ISM in the younger interval (Figs. 4 and 5). The termination of the YD event at ~11.3 kyr BP at Umsynrang cave is probably due to an age uncertainty in the present study. Earlier cave records from the nearby Mawmluh cave and eastern Himalaya precipitation reconstruction also indicate a short event of weak monsoon during ~11.5–11.3 kyr BP (Figs. 4iii, 5ii, 5iii, 6ii), possibly linked to the existence of short-lived cold pulses in the North Atlantic (Fig. 4vii) (Ali et al., 2018; Andersen et al., 2004; Berkelhammer et al., 2012; Dutt et al., 2015), which is also reflected in the PC1 time series (Fig. 9).

4.3. Post YD (~11.3–10.1 kyr BP)

There is a general long term increase in summer monsoon precipitation between ~ 11.3 and 10.1 kyr BP with high-frequency shifts in the ISM (Figs. 4–6) suggested by high amplitude variability in PC time series of this interval (Fig. 10). The strengthening of the AMOC and westerlies jet stream may have caused northward migration of the ITCZ and increased monsoon precipitation in the Indian subcontinent (Enzel et al., 1999; Gupta et al., 2013). Various marine, lacustrine and terrestrial records from as well as beyond the Indian subcontinent also suggest stronger summer monsoon during the early Holocene (Fleitmann et al., 2003; Ali et al., 2018; Dixit et al., 2014; Wu et al., 2018). The resumption of strong AMOC and warming of NH reduced the influence of westerly jet stream and enhanced land-sea heat contrast.

During the early Holocene, the Umsynrang cave $\delta^{18}O$ value associated with Mawmluh and Chinese cave remains the same, but it is also associated and positively correlated with the Liang Luar cave $\delta^{18}O$ values. The Sofular cave associated with WP SST has an inverse correlation with the Umsynrang cave $\delta^{18}O$ values (Fig. 8; Table 4s). The Sofular cave record also suggests weakened westerlies as a result of atmospheric warming in NH (Fig. 8). NGRIP data (Fig. 4vii) suggests the warming of the North Atlantic Ocean during the early Holocene that marks the decreased influence of the mid-latitude westerlies on the tropical monsoon systems (Wang et al., 2001; Anderson et al., 2004; Dutt et al., 2015). The interval between 10.8 and 10.1 kyr BP observed high frequency pronounced abrupt shifts in the ISM (Fig. 10), the most prominent of which

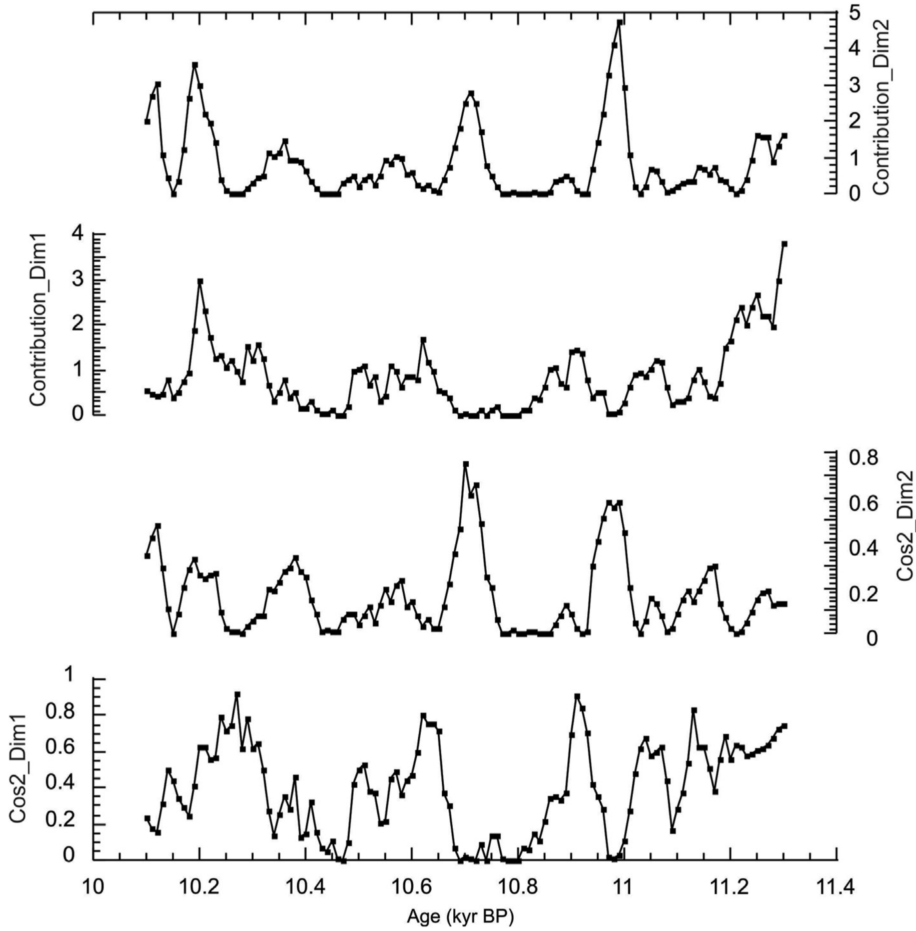

Fig. 10. The time series plot of Cos2 and Contribution value of dimension 1 (Dim1 or PC1) and dimension 2 (Dim2 or PC2) for the period between 11.3 and 10.1 kyr BP.

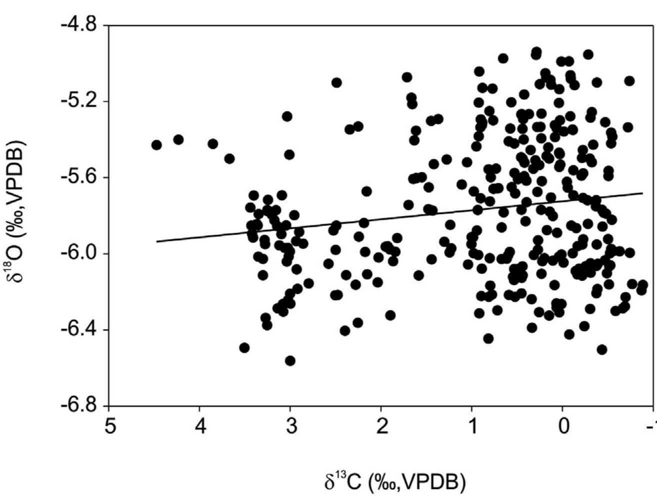

Fig. 11. Hendy test correlation between δ^{18}O and δ^{13}C time series for the whole data from the Umsynrang cave, northeastern India.

occurred during ~10.8 to 10.6 kyr BP (Figs. 4 and 5). The Kalakot cave δ^{18}O values representing westerlies intensity also show high amplitude fluctuation during the early Holocene (Fig. 6vii). This event is omnipresent in high-resolution records of ISM variability in the South Asian region (Figs. 4 and 5). The SST record over EAS, BoB and WP shows an overall increasing trend but does not have one to one correlation with the ISM intensification (Fig. 6iv, 6v, 6vi), which is further confirmed by the PCA and Pearson correlation analysis (Fig. 8; Tables 2s and 4s). The significant abundance of upwelling indicator *G. bulloides* in the western Arabian Sea further supports enhanced monsoonal wind (Fig. 6iii; Gupta et al., 2013), but did not have significant teleconnections with the equatorial western Pacific SST till 10.1 kyr BP as proposed by Gill et al. (2017). The δ^{13}C value is reflecting the significant vegetation growth similar to modern condition during the period of higher ISM precipitation (Lechleitner et al., 2017). The drip rate in northeastern India cave does not directly reflect the amount of precipitation, but increases during and after the summer monsoon. The saturation of the water reservoir plays a significant role and a saturated epikarst reservoir can cause higher drip discharge (Breitenbach et al., 2015). The frequent higher ISM precipitation saturated the epikarst reservoir and caused higher growth of the stalagmite during the early Holocene.

The strong/weak ISM intensity generally follows the periods of intense cooling/warming in the North Atlantic, respectively (Fig. 4vii). The Southern Hemisphere (SH) rapid warming may have caused reduced ISM precipitation. The ITCZ position governs the extent of monsoonal precipitation over the south Asian region and is very sensitive to a marginal shift in the atmospheric energy balance. The stronger transport of atmospheric energy towards the north, shifted the ITCZ southwards during the YD, while during the early Holocene, boreal summer (Loutre, 2009) transported the atmospheric energy southwards that caused farther northward migration of the ITCZ and thus caused higher precipitation

(Schneider et al., 2014). Various climate models, as well as paleoclimate proxies, suggest that the early Holocene ISM strengthening (Overpeck et al., 1996; Gupta et al., 2003, 2005, 2013; Ali et al., 2018) and also related to reduced snow cover over Tibetan Plateau (Marzin and Braconnot, 2009; Dixit et al., 2014).

5. Conclusions

Proxy record from Umsynrang cave suggests high Indian summer monsoon precipitation in northeastern India during ~15.4 to 12.9 kyr BP (B-Å period) and ~11.3 to 10.1 kyr BP (early Holocene) with high-frequency shifts in the latter interval. The Indian Summer Monsoon (ISM) strength weakened during ~12.9–11.3 kyr BP (Younger Dryas or YD cold event) as a result of the weakening of the Atlantic Meridional Overturning Circulation (AMOC) and strengthening of the westerlies. The position of the Inter-Tropical Convergence Zone (ITCZ) modulated ISM variability and it periodically shifted towards the equator or SH during the YD. The AMOC, westerly jet stream and land-sea heat contrast influenced the ISM precipitation during the YD. Northern Hemisphere atmospheric warming shifts the ITCZ northward caused enhanced precipitation. However, a high-frequency shift in ISM precipitation was observed during the early Holocene. Sea surface temperature over the western Pacific did not have direct teleconnections with the ISM during the YD and early Holocene until 10.1 kyr BP.

Authors contributions

RKS proposed the problem, collected the samples, did subsampling interpreted the results and wrote the initial draft of the manuscript. HC and GK generated the Uranium–Thorium series dating of samples and SC generated stable isotope data. AKG helped in data interpretation, writing and finalization of the manuscript. SD, HC, GK and SC helped in data interpretation and writing of the manuscript.

Submission declaration and verification

The article has not been published previously and it is not under consideration for publication elsewhere. The publication is approved by all authors and tacitly or explicitly by the responsible authorities where the work was carried out, and that, if accepted, it will not be published elsewhere in the same form, in English or in any other language, including electronically without the written consent of the copyright-holder.

Declaration of competing interest

The authors declare that there is no conflict of interests.

Acknowledgements

RKS, AKG, SD thank the WIHG for providing infrastructure facilities during this work. AKG thanks the Department of Science and Technology, New Delhi for funding under J.C. Bose fellowship (Grant no. SR/S2/JCB-80/2011). RKS acknowledged support and help of Dr. Jayendra Singh of WIHG during the sampling and financial support from IIT Bhubaneswar (SP-53) and MoES (RP-077). WIHG provided the infrastructure and necessary facilities to carry out this research. We acknowledge Brian D. Kharpran Daly and Gregory Diengdoh for their logistic help and Daniel Gebauer for assistance during the field work and sample collection. We are grateful to Editor Miryam Bar-Matthews and three anonymous reviewers for their constructive suggestions that significantly improved the manuscript.

Appendix A. Supplementary data

Supplementary data to this article can be found online at https://doi.org/10.1016/j.quascirev.2021.106888.

References

Ali, S.N., Dubey, J., Ghosh, R., Quamar, M.F., Sharma, A., Morthekai, P., Dimri, A.P., Shekhar, M., Arif, Md., Agrawal, S., 2018. High frequency abrupt shifts in the Indian summer monsoon since Younger Dryas in the Himalaya. Sci. Rep. 8 (1), 1–8.

Andersen, K., Azuma, N., Barnola, J., et al., 2004. High-resolution record of Northern Hemisphere climate extending into the last interglacial period. Nature 431. https://doi.org/10.1038/nature02805.

Berkelhammer, M., Sinha, A., Stott, L., Cheng, H., Pausata, F.S.R., Yoshimura, K., 2012. An abrupt shift in the Indian monsoon 4000 Years ago. In: Giosan, L., et al. (Eds.), Climates, Landscapes, and Civilizations: American Geophysical Monograph 198, pp. 75–87. https://doi.org/10.1029/2012GM001207.

Breitenbach, S., 2009. Changes in Monsoonal Precipitation and Atmospheric Circulation during the Holocene Reconstructed from Stalagmites from Northeastern India. PhD Thesis. University of Postdam, Germany.

Breitenbach, S.F.M., Adkins, J.F., Meyer, H., Marwan, N., Kumar, K.K., Haug, G.H., 2010. Strong influence of water vapor source dynamics on stable isotopes in precipitation observed in Southern Meghalaya, NE India. Earth Planet Sci. Lett. 292, 212–220. https://doi.org/10.1016/j.epsl.2010.01.038.

Breitenbach, S.F.M., Lechleitner, F.A., Meyer, H., Diengdoh, G., Mattey, D., Marwan, N., 2015. Cave ventilation and rainfall signals in dripwater in a monsoonal setting–a monitoring study from NE India. Chem. Geol. 402, 111–124.

Bond, G., Kromer, B., Beer, J., Muscheler, R., Evans, M.N., Showers, W., Bonani, G., 2001. Persistent solar influence on North Atlantic climate during the Holocene. Science 294 (5549), 2130–2136.

Cheng, H., Edwards, R.L., Broecker, W.S., Denton, G.H., Kong, X., Wang, Y., Zhang, R., Wang, X., 2009. Ice age terminations. Science 326 (5950), 248–252.

Cheng, H., Edwards, R.L., Shen, C.C., Polyak, V.J., Asmerom, Y., Woodhead, J., et al., 2013. Improvements in ^{230}Th dating, ^{230}Th and ^{234}U half-life values, and U–Th isotopic measurements by multi-collector inductively coupled plasma mass spectrometry. Earth Planet Sci. Lett. 371–372, 82–91. https://doi.org/10.1016/j.epsl.2013.04.006.

Cheng, H., Edwards, R.L., Sinha, A., Spötl, C., Yi, L., Chen, S., et al., 2016. The Asian monsoon over the past 640,000 years and ice age terminations. Nature 534 (7609), 640.

Cheng, H., Zhang, H., Spötl, C., Baker, J., Sinha, A., Li, H., Bartolomé, M., Moreno, A., Kathayat, G., Zhao, J., Dong, X., 2020. Timing and structure of the Younger Dryas event and its underlying climate dynamics. Proc. Natl. Acad. Sci. Unit. States Am. 117 (38), 23408–23417.

Condron, A., Winsor, P., 2012. Meltwater routing and the younger Dryas. Proc. Natl. Acad. Sci. Unit. States Am. 109 (49), 19928–19933.

Dang, H., Jian, Z., Bassinot, F., Qiao, P., Cheng, X., 2012. Decoupled Holocene variability in surface and thermocline water temperatures of the Indo-pacific warm pool. Geophys. Res. Lett. 39 (1), GL051054.

Dansgaard, W., White, J.W.C., Johnsen, S.J., 1989. The abrupt termination of the Younger Dryas climate event. Nature 339 (6225), 532.

Das, M., Singh, R.K., Holbourn, A., Farooq, S.H., Vats, N., Pandey, D.K., 2021. Paleoceanographic evolution of the Japan Sea during the Pleistocene–A benthic foraminiferal perspective. Palaeogeogr. Palaeoclimatol. Palaeoecol. 566, 110238.

Dixit, Y., Hodell, D.A., Petrie, C.A., 2014. Abrupt weakening of the summer monsoon in northwest India̋ 4100 yr ago. Geology 42 (4), 339–342.

Dreybrodt, W., 2008. Evolution of the isotopic composition of carbon and oxygen in a calcite precipitating H_2O–CO_2–$CaCO_3$ solution and the related isotopic composition of calcite in stalagmites. Geochem. Cosmochim. Acta 72 (19), 4712–4724.

Dutt, S., Gupta, A.K., Clemens, S.C., Cheng, H., Singh, R.K., Kathayat, G., Edwards, R.L., 2015. Abrupt changes in Indian summer monsoon strength during 33,800 to 5500 years B.P. Geophys. Res. Lett. 42, 5526–5532. https://doi.org/10.1002/2015GL064015.

Dutt, S., Gupta, A.K., Cheng, H., Clemens, S.C., Singh, R.K., Tewari, V.C., 2021. Indian summer monsoon variability in northeastern India during the last two millennia. Quat. Int. 571, 73–80.

Dykoski, C.A., Edwards, R.L., Cheng, H., Yuan, D., Cai, Y., Zhang, M., et al., 2005. A high-resolution, absolute-dated Holocene and deglacial Asian monsoon record from Dongge Cave, China. Earth Planet Sci. Lett. 233 (1–2), 71–86.

Enzel, Y., Ely, L.L., Mishra, S., Ramesh, R., Amit, R., Lazar, B., et al., 1999. High-resolution Holocene environmental changes in the thar desert, northwestern India. Science 284 (5411), 125–128.

Fleitmann, D., Burns, S.J., Mudelsee, M., Neff, U., Kramers, J., Mangini, A., et al., 2003. Holocene forcing of the Indian monsoon recorded in a stalagmite from southern Oman. Science 300 (5626), 1737–1739.

Fleitmann, D., Cheng, H., Badertscher, S., Edwards, R.L., Mudelsee, M., Göktürk, O., et al., 2009. Timing and climatic impact of Greenland interstadials recorded in stalagmites from northern Turkey. Geophys. Res. Lett. 36 (19).

Gautam, P.K., Narayana, A.C., Band, S.T., Yadava, M.G., Ramesh, R., Wu, C.C., et al., 2019. High-resolution reconstruction of Indian summer monsoon during the

Bølling-Ållerød from a central Indian stalagmite. Palaeogeogr. Palaeoclimatol. Palaeoecol. 514, 567–576.
Gill, E.C., Rajagopalan, B., Molnar, P.H., Kushnir, Y., Marchitto, T.M., 2017. Reconstruction of Indian summer monsoon winds and precipitation over the past 10,000 years using equatorial pacific SST proxy records. Paleoceanography 32 (2), 195–216.
Griffiths, M.L., Drysdale, R.N., Gagan, M.K., Zhao, J.X., et al., 2009. Increasing Australian–Indonesian monsoon rainfall linked to early Holocene sea-level rise. Nat. Geosci. 2 (9), 636–639.
Gupta, A.K., Anderson, D.M., Overpeck, J.T., 2003. Abrupt changes in the Asian southwest monsoon during the Holocene and their links to the north Atlantic Ocean. Nature 421 (6921), 354.
Gupta, A.K., Das, M., Anderson, D.M., 2005. Solar influence on the Indian summer monsoon during the Holocene. Geophys. Res. Lett. 32 (17).
Gupta, A.K., Dutt, S., Cheng, H., Singh, R.K., 2019. Abrupt changes in Indian summer monsoon strength during the last~ 900 years and their linkages to socio-economic conditions in the Indian subcontinent. Palaeogeogr. Palaeoclimatol. Palaeoecol. 536, 109347.
Gupta, A.K., Mohan, K., Das, M., Singh, R.K., 2013. Solar forcing of the Indian summer monsoon variability during the Ållerød period. Sci. Rep. 3, 2753.
Hendy, C.H., 1971. The isotopic geochemistry of speleothems—I. The calculation of the effects of different modes of formation on the isotopic composition of speleothems and their applicability as palaeoclimatic indicators. Geochem. Cosmochim. Acta 35, 801–824.
Huguet, C., Routh, J., Fietz, S., Lone, M.A., Kalpana, M.S., Ghosh, P., et al., 2018. Temperature and monsoon tango in a tropical stalagmite: last glacial-interglacial climate dynamics. Sci. Rep. 8 (1), 5386.
Kassambara, A., 2017. Practical Guide to Principal Component Methods in R: PCA, M (CA), FAMD, MFA, HCPC, Factoextra, vol. 2. Sthda.
Kathayat, G., Cheng, H., Sinha, A., Berkelhammer, M., Zhang, H., Duan, P., et al., 2018. Evaluating the timing and structure of the 4.2 ka event in the Indian summer monsoon domain from an annually resolved speleothem record from Northeast India. Clim. Past 14 (12), 1869–1879.
Kharpran Daly, B.D., 2006. The Caves of Meghalaya. The Directorate of Information and Public Relations, Government of Meghalaya, Shillong.
Köhler, P., Knorr, G., Buiron, D., Lourantou, A., Chappellaz, J., 2011. Abrupt rise in atmospheric CO_2 at the onset of the Bølling/Allerød: in-situ ice core data versus true atmospheric signal. Clim. Past 7 (2), 473–486.
Kotlia, B.S., Singh, A.K., Sanwal, J., Raza, W., Ahmad, S.M., Joshi, L.M., Sirohi, M., Sharma, A.K., Sagar, N., 2016. Stalagmite inferred high resolution climatic changes through Pleistocene-Holocene transition in Northwest Indian Himalaya. J. Earth Sci. Climatic Change 7 (338), 1000338.
Lê, S., Josse, J., Husson, F., 2008. FactoMineR: an R package for multivariate analysis. J. Stat. Software 25 (1), 1–18.
Lechleitner, F.A., Breitenbach, S.F., Cheng, H., Plessen, B., Rehfeld, K., Goswami, B., et al., 2017. Climatic and in-cave influences on $\delta^{18}O$ and $\delta^{13}C$ in a stalagmite from northeastern India through the last deglaciation. Quat. Res. 88 (3), 458–471.
Loutre, M.F., 2009. Precession, climatic. In: Gornitz, V. (Ed.), Encyclopedia of Paleoclimatology and Ancient Environments. Springer, Dordrecht, pp. 825–826.
Marzin, C., Braconnot, P., 2009. The role of the ocean feedback on Asian and African monsoon variations at 6 kyr and 9.5 kyr BP. Compt. Rendus Geosci. 341 (8–9), 643–655.
Mayewski, P.A., Meeker, L.D., Whitlow, S., Twickler, M.S., Morrison, M.C., Alley, R.B., et al., 1993. The atmosphere during the younger Dryas. Science 261 (5118), 195–197.
Mishra, P.K., Anoop, A., Schettler, G., Prasad, S., Jehangir, A., Menzel, P., et al., 2015. Reconstructed late Quaternary hydrological changes from lake Tso Moriri, NW Himalaya. Quat. Int. 371, 76–86.
Murata, F., Hayashi, T., Matsumoto, J., Asada, H., 2007. Rainfall on the Meghalaya plateau in northeastern India—one of the rainiest places in the world. Nat. Hazards 42 (2), 391–399.
Myers, C.G., Oster, J.L., Sharp, W.D., Bennartz, R., Kelley, N.P., Covey, A.K., et al., 2015. Northeast Indian stalagmite records Pacific decadal climate change: implications for moisture transport and drought in India. Geophys. Res. Lett. 42 (10), 4124–4132.
Neff, U., Burns, S.J., Mangini, A., Mudelsee, M., Fleitmann, D., Matter, A., 2001. Strong coherence between solar variability and the monsoon in Oman between 9 and 6 kyr ago. Nature 411 (6835), 290.
North Greenland Ice Core Project Members, 2004. High-resolution record of Northern Hemisphere climate extending into the last interglacial period. Nature 431, 147–151.
Overpeck, J., Anderson, D., Trumbore, S., Prell, W., 1996. The southwest Indian Monsoon over the last 18 000 years. Clim. Dynam. 12 (3), 213–225.
Panmei, C., Divakar Naidu, P., Mohtadi, M., 2017. Bay of Bengal exhibits warming trend during the younger Dryas: implications of AMOC. G-cubed 18 (12), 4317–4325.
Parthasarathy, B., Kumar, K.R., Munot, A.A., 1993. Homogeneous Indian monsoon rainfall: variability and prediction. Proc. Indian Acad. Sci. Earth Planet Sci. 102 (1), 121–155.
Partin, J.W., Quinn, T.M., Shen, C.C., Okumura, Y., Cardenas, M.B., Siringan, F.P., et al., 2015. Gradual onset and recovery of the Younger Dryas abrupt climate event in the tropics. Nat. Commun. 6, 8061.
Paillard, D., Labeyrie, L., Yiou, P., 1996. Macintosh program performs time-series analysis. Eos, Trans. Am. Geophys. Union 77 (39).
R Core Team, 2017. R: A Language and Environment for Statistical Computing. R Foundation for Statistical Computing, Vienna, Austria. https://www.R-project.org/.
Rawat, S., Gupta, A.K., Srivastava, P., Sangode, S.J., Nainwal, H.C., 2015. A 13,000 year record of environmental magnetic variations in the lake and peat deposits from the Chandra valley, Lahaul: implications to Holocene monsoonal variability in the NW Himalaya. Palaeogeogr. Palaeoclimatol. Palaeoecol. 440, 116–127.
Saraswat, R., Lea, D.W., Nigam, R., Mackensen, A., Naik, D.K., 2013. Deglaciation in the tropical Indian Ocean driven by interplay between the regional monsoon and global teleconnections. Earth Planet Sci. Lett. 375, 166–175.
Schlolaut, G., Brauer, A., Nakagawa, T., Lamb, H.F., Tyler, J.J., Staff, R.A., et al., 2017. Evidence for a bi-partition of the younger Dryas Stadial in East Asia associated with inversed climate characteristics compared to Europe. Sci. Rep. 7, 44983.
Schneider, T., Bischoff, T., Haug, G.H., 2014. Migrations and dynamics of the intertropical convergence zone. Nature 513 (7516), 45–53.
Schulz, H., von Rad, U., Erlenkeuser, H., 1998. Correlation between Arabian Sea and Greenland climate oscillations of the past 110,000 years. Nature 393 (6680), 54–57.
Scholz, D., Hoffmann, D.L., 2011. StalAge–An algorithm designed for construction of speleothem age models. Quat. Geochronol. 6 (3–4), 369–382.
Shindell, D.T., Schmidt, G.A., Mann, M.E., Rind, D., Waple, A., 2001. Solar forcing of regional climate change during the Maunder Minimum. Science 294 (5549), 2149–2152.
Sinha, A., Cannariato, K.G., Stott, L.D., Li, H.C., You, C.F., Cheng, H., et al., 2005. Variability of Southwest Indian summer monsoon precipitation during the Bølling-Allerød. Geology 33 (10), 813–816.
Thiagarajan, N., Subhas, A.V., Southon, J.R., Eiler, J.M., Adkins, J.F., 2014. Abrupt pre-Bølling–Allerød warming and circulation changes in the deep ocean. Nature 511 (7507), 75.
Thompson, L.G., Yao, T., Mosley-Thompson, E., Davis, M.E., Henderson, K.A., Lin, P.N., 2000. A high-resolution millennial record of the South Asian monsoon from Himalayan ice cores. Science 289 (5486), 1916–1919.
Tiwari, S.K., Singh, R.K., Singh, J., Gupta, A.K., Bartarya, S.K., Rai, S.K., 2015. Impact of limestone mining activities on major ion geochemistry of Krem Markhyrdop water, Meghalaya, India. Himal. Geol. 36 (1), 74–80.
Wang, Y.J., Cheng, H., Edwards, R.L., An, Z.S., Wu, J.Y., Shen, C.C., et al., 2001. A high-resolution absolute-dated late Pleistocene monsoon record from Hulu Cave, China. Science 294 (5550), 2345–2348.
Wiedner, E., Scholz, D., Mangini, A., Polag, D., Mühlinghaus, C., Segl, M., 2008. Investigation of the stable isotope fractionation in speleothems with laboratory experiments. Quat. Int. 187 (1), 15–24.
Wu, D., Chen, X., Lv, F., Brenner, M., Curtis, J., Zhou, A., Chen, J., Abbott, M., Yu, J., Chen, F., 2018. Decoupled early Holocene summer temperature and monsoon precipitation in southwest China. Quat. Sci. Rev. 193, 54–67.
Wünnemann, B., Demske, D., Tarasov, P., Kotlia, B.S., Reinhardt, C., Bloemendal, J., et al., 2010. Hydrological evolution during the last 15 kyr in the Tso Kar lake basin (Ladakh, India), derived from geomorphological, sedimentological and palynological records. Quat. Sci. Rev. 29 (9–10), 1138–1155.
Yancheva, G., Nowaczyk, N.R., Mingram, J., Dulski, P., Schettler, G., Negendank, J.F., et al., 2007. Influence of the intertropical convergence zone on the East Asian monsoon. Nature 445 (7123), 74.
Yuan, D., Cheng, H., Edwards, R.L., Dykoski, C.A., Kelly, M.J., Zhang, M., et al., 2004. Timing, duration, and transitions of the last interglacial Asian monsoon. Science 304 (5670), 575–578.